# Title:

# High Spatial Resolution Ambient Ionization Mass Spectrometry Imaging Using Microscopy Image Fusion

Chih-Lin Chen, Li-En Lin, Ying-Chen Huang, Hsin-Hsiang Chung, Ko-Chien Chen, Yu-Ju Peng, Chiao-Wei Lin, Shih-Torng Ding, Tang-Long Shen, Cheng-Chih Hsu*

**Author information**

Chih-Lin Chen, Li-En Lin

These authors contributed equally to this work.

Affiliations

Department of Chemistry, National Taiwan University, No. 1, Sec. 4, Roosevelt Rd., Taipei 10617, Taiwan (R.O.C.)

Chih-Lin Chen, Li-En Lin, Ying-Chen Huang, Hsin-Hsiang Chung

Department of Plant Pathology and Microbiology, National Taiwan University, No. 1, Sec. 4, Roosevelt Rd., Taipei 10617, Taiwan (R.O.C.)

Ko-Chien Chen, Tang-Long Shen

Department of Animal Science and Technology, National Taiwan University, No. 1, Sec. 4, Roosevelt Rd., Taipei 10617, Taiwan (R.O.C.)

Yu-Ju Peng, Chiao-Wei Lin, Shih-Torng Ding

Department of Life Science, National Taiwan University, No. 1, Sec. 4, Roosevelt Rd., Taipei 10617, Taiwan (R.O.C.)

Chiao-Hui Hsieh, Hsueh-Fen Juan

**Corresponding author**

Correspondence to Cheng-Chih Hsu.

**Abstract**

Mass spectrometry imaging (MSI) using ambient ionization technique enables a direct chemical investigation of biological samples with minimal sample pretreatment. However, detailed morphological information of the sample is often lost due to its limited spatial resolution. We demonstrated that the fusion of ambient ionization MSI with optical microscopy of routine hematoxylin and eosin (H&E) staining produces predictive, high-resolution molecular imaging. In this study, desorption electrospray ionization (DESI) and nanospray desorption electrospray ionization (nanoDESI) mass spectrometry were employed to visualize lipid and protein species on mouse tissue sections. The resulting molecular distributions obtained by ambient ionization MSI-microscopy fusion were verified with matrix-assisted laser desorption ionization time-of-flight (MALDI-TOF) MSI and routine immunohistochemistry (IHC) staining on the adjacent sections. Label-free molecular imaging with 5-µm spatial resolution can be achieved using DESI and nanoDESI, whereas the typical spatial resolution of ambient ionization MSI is ~100 µm. In this regard, sharpened molecular histology of tissue sections was achieved, providing complementary references to the pathology. Such multi-modality integration enabled the discovery of potential tumor biomarkers. After image fusion, we identified about 70% more potential biomarkers that could be used to determine the tumor margins on a lung tissue section with metastatic tumors.

**Introduction**

Image fusion combining spatially-resolved data from multiple analytical tools has been utilized to generate high quality images for better human interpretation[1]. A variety of image fusion methods, based on wavelet transform, morphology knowledge, artificial neural network, multivariate regression, and Pan-Sharpening methods, has been developed and were successfully applied in different scientific fields[1–4]. For instance, it has been largely used for remote sensing and object recognition by merging the satellite imaging with high resolution panchromatic image to harvest more information[1,5]. One of the other successful applications of imaging fusion is in merging complementary medical images obtained with multiple modalities into one highly defined image for clinical analysis[4,6].

Mass spectrometry imaging (MSI) provides spatially resolved chemical information of the surface of biological samples in a label-free manner, and has been profoundly used in preclinical, pharmaceutical and biological studies[7–15]. Furthermore, ambient ionization mass spectrometry imaging methods are capable of providing spatially resolved chemical information of cells and tissues with minimal sample pretreatment under atmospheric condition. In specific, the biological tissue sections that used for conventional pathological and molecular staining can be directly implemented for ambient ionization MSI at their intact states. Desorption electrospray ionization (DESI) and nanospray-desorption electrospray ionization (nanoDESI), were two of the most commonly used ambient ionization methods for *in-situ* analysis for different classes of compounds [10,11,16–22]. MSI using DESI and nanoDESI is of great potential as a complementary tool for pathological examinations in cancer diagnosis and has been largely used in determining the tumor margins[23–26]. In previous reports, lipid species had been widely studied and were served as important biomarkers to identify the malignant and benign tumor tissue by DESI MSI[23,24]. On the other hand, proteins were also reported to discriminate between normal tissues and tumors using nanoDESI MSI[26]. However, one of the challenges for clinical study by DESI and nanoDESI MSI is its spatial resolving power [27–30].

To visualize fine chemical details of the sample surface in its intact state comparable with conventional optical microscopy-based methods, the spatial resolution of ambient ionization MSI requires to improve[31]. Several instrumental approaches to increase the spatial resolution of ambient ionization MSI have been reported. For example, a hybrid atomic force microscopy mass spectrometer was applied for mapping bacterial colonies at sub-micrometer level under atmospheric pressure[32]. On the other hand, laser desorption/ablation-based methods allow imaging at subcellular level[33,34]. DESI is currently the most widely recognized ambient ionization methods for MSI. Although its lateral resolution can reach to about 10 μm with optimal parameter settings[35], the typical resolution of DESI MSI is about 100 μm. NanoDESI is known for its ability of *in-situ* protein MSI [10,11], but its spatial resolution is restricted by the instrumental design and occasional carried-over among pixels.

In addition to the instrumental approaches, numerical approaches, image fusion in particular, is an alternative strategy to surpass the inherent limitation of each ionization methods. Such strategy allows us to achieve a higher spatial resolution without using custom instruments or specialized experimental setup. Recently, Multivariate regression image fusion of optical microscopy data with ultrahigh vacuum-based MSI, including matrix-assisted laser desorption ionization (MALDI) and secondary ion mass

spectrometry (SIMS) MSI, were reported to achieve sharpened molecular imaging with spatial resolution at cellular level on tissue sections[36,37]. approach for image fusion was reported to be broadly applicable to different tissue type. The distribution of ions was clear at the sub-cellular level. Sharped ion images of MALDI mass spectrometry fused with microscopy of mouse tissue sections were shown in their study[37]. In addition, fusion of SIMS and electron microscopy images were also reported[38]. Although high resolution molecular distribution were revealed, these mass spectrometry methods operated under high vacuum, which limits the compatibility with conventional imaging methods for pathological examinations.

In our study, an optical microscope was applied to obtain images containing meticulous details of H&E stained tissue sections. Using multivariate regression algorithm, we fused MSI with optical microscopy and generated predictive fine-grained MSI. This method was applied in different tissue types and demonstrated as a tool for cancer diagnosis. By combining optical microscopy with ambient ionization methods, DESI, and nanoDESI, for tissue mapping with image fusion, both the image resolution and image quality were greatly improved. The workflow of our study is shown in Fig. 1.

## Results

**Elevating spatial resolution of lipid species mapping in DESI MSI.** The results for fusion of DESI MSI for mouse brain and cerebellum coronal sections were shown in Fig. 2, whereas the results for mouse kidney sections were shown in Fig. 3. In Fig. 2, the distribution of two phospholipids species, phosphatidylethanolamine (PE P-18:0/20:5) and phosphatidylcholine (PC 18:0/20:1) at *m/z* 772.5 and 838.6, respectively, were revealed by our raw DESI MSI at 150-mm resolution. PE (P-18:0/20:5) were largely found in the grey matter, whereas PC (18:0/20:1) were measured in the white matter. Similar distributions of these two phospholipids species in mammalian brains have been reported using DESI MSI[39,40]. In Fig. 3, PE (P-18:0/20:5) and PC (16:0/16:0) distributed in cortex, while the PC (16:0/18:1) distributed in the medulla of the kidney. These results were also similar to the previous studies[41,42]. Although the DESI MSI provided a molecular imaging at sub-tissue level, in which different lipid species

showed a drastic difference in their distribution in the brain, morphological details that can be readily obtained with a laboratory optical microscope, were missing due to its limitation in spatial resolution. After the fusion of DESI MSI with the optical microscopic image of the H&E staining using the same tissue sections, predictive molecular imaging of the denoted phospholipids were generated, showing much improved morphological details compared with the raw DESI MSI. For example, the distribution of PE (P-18:0/20:5) from the raw DESI MSI only roughly revealed the hippocampus while the predictive image shows that PE (P-18:0/20:5) has lower abundance in the dentate gyrus. In the case of cerebellum, the originally pixelated molecular imaging was sharpened by image fusion, distinguishing between the cerebellar cortex and medulla. For the kidney sections in Fig. 3, clear boundaries between the outer stripe of the outer medulla (OSOM) and the inner stripe of the outer medulla (ISOM) were shown after image fusion.

**High-quality protein imaging by fusion of nanoDESI MSI.** Unlike DESI, nanoDESI utilizes a micro-liquid junction sustained between two fused silica capillaries to desorb analyte compounds from the sample surfaces. This allows nanoDESI MS to detect large biomolecules, e.g. proteins, with molecular weight up to 15 kDa[11,17,43]. However, as the stability of the micro-junction is sensitive to the flatness of the tissue sections, the carry-over of the analyte compounds among neighboring pixels in nanoDESI MSI is thus more significant than in DESI MSI, causing artifacts to the images and making it challenging to interpret. To expand the utility of image fusion to protein imaging, we applied nanoDESI MSI to mice tissue sections. In Fig. 4, the spatial distribution of peak *m/z* 785.55 (+18 charge), annotated as myelin basic protein (MBP) using top-down tandem mass analysis (Supplementary Figure 4), was largely found on mice brain and mapped by nanoDESI MSI. Similar to the previous report , as MBP is highly expressed in the myelinated axons, it was profoundly observed in the white matter of the brain (Fig. 4b)[11]. After image fusion with

the H&E stained adjacent section, a high-resolution image of MBP was thus generated (Fig. 4c). Remarkably, the severe tailing and cross-contamination of ion signals in the raw nanoDESI MSI due to carryover effect was significantly eliminated in the predictive image. The distribution of MBP is well sharpened and in agreement with the histological features of the mice brain section. In order to prove the genuineness of the prediction using image fusion, a high resolution MALDI-TOF MSI was also implemented to the second adjacent sections. The result of MALDI-TOF MSI (Fig. 4d) shows a very high similarity with the predictive image and thus verified that the pixel-wised carry-over was efficiently removed.

In addition, the spatial distribution of hemoglobin subunit alpha (*m/z* 751.40) was successfully mapped in sagittal and coronal kidney sections as shown in Fig. 4f (Top-down analysis was shown in Supplementary Figure 5). The predictive image after fusion with H&E stained sections exhibit that a large amount of hemoglobin subunit alpha was still located in the blood vessels and not smeared during the cryosectioning. The high-resolution MALDI-TOF MSI of the adjacent sections also verified this observation. Due to the fact that the histological features of kidney change after few sections, a slight difference of the protein distribution obtained by nanoDESI MSI-microscopy fusion and MALDI-TOF MSI are expected.

**Confirmation of predicted MSI by conventional methods.** We have demonstrated that DESI/nanoDESI MSI-microscopy image fusion provides an ability to resolve the molecular distribution of biomolecules on tissue sections at cellular level (5-µm), which is comparable with the traditional immunohistochemical approaches. However, immunohistochemistry (IHC) staining requires pre-requisite knowledge to the target compounds, proteins in specific, and do not allows label-free analysis. Thus, to further demonstrate the capability of DESI/nanoDESI MSI-microscopy image fusion in resolving the distribution of biomolecules in a

label-free manner, a series of adjacent mouse brain sections were prepared and sequentially analyzed (1) DESI, (2) nanoDESI MSI-microscopy fusion, (3) MALDI-TOF MSI, and (4) IHC staining microcopy for lipid and protein imaging (Fig. 5).

For lipid detection, the *m/z* 772.5 (PE(P-18:0/20:5)) was observed in the region of the cerebral cortex by DESI imaging. However, the boundary of PE(P-18:0/20:5) was blurred and unclear by DESI MSI (Fig. 5a) compared to the MALDI-TOF MSI (Fig. 5c). Meanwhile, after image fusion was incorporated, the structure of the brain section was resolved in the predictive high spatial resolution molecular image (Fig. 5b). For example, the hippocampus were unambiguously sketched in the mapping of PE(P-18:0/20:5), showing comparable results with the MALDI-TOF MSI.

For protein detection, MBP (*m/z* 744.21, +19 charge) was visualized by nanoDESI MSI. The nominal spatial resolution (determined by the speed of translational stage and rate of data collection) of raw nanoDESI MSI was 200 μm, and the tissue histological details was relatively difficult to recognize due to the limited spatial resolution due to the large microjunction radius and carry-over. In the raw nanoDESI MSI (Fig. 5e), the histochemical relationship of MBP was ambiguous, especially at the brain stem area. In Fig. 5i, the images at the retrosplenial cortex and the midbrain are enlarged. After image fusion of the data, MBP was predicted to be localized at the fiber tracts and fasciculus retroflexus (fr). Similar results were obtained with MALDI MSI (Supplementary Figure 7). MBP is one of a major component of the myelin sheath. As a result, MBP can be easily detected in the white matter of a brain. To verify the result obtained our nanoDESI MSI, high-resolution microscopic image of MBP was obtained by IHC staining of the neighboring tissue[44]. Unambiguously, we were able to observe analogous distributions of MBP from the results of nanoDESI MSI-microscopy image fusion and the conventional IHC staining, while eliminating complex and time-consuming sample pretreatment and the need for specific antibodies.

**Image fusion of DESI MSI applied to cancer diagnosis.** MSI had been widely applied to study several cancer models[23–27,45,46]. By targeting specific biomarkers or comparing chemical profiles of different tissue margins, we were able to delineate cancerous margin on a heterogeneous tissue. Although ambient ionization MSI provides simple and rapid molecular evaluation of clinical specimens[47], the spatial resolution often limits the performance in assessing the cancerous margin, especially at the early stage or metastatic cancer. Failure in discerning cancer cells from benign tissue increase the likelihood of requiring a second operation[48]. Thus, we seek to implement DESI MSI-microscopy image fusion for observing detailed molecular distribution.

To confirm the capability of predicting precise cancerous margin, we applied image fusion to obtain fine spatial resolution molecular imaging in breast cancer metastatic lung tissue section (Fig. 6). To validate whether the ion's distribution in MSI correlated with the cancer region on the tissue section, the receiver operating characteristic (ROC) curve was plotted for each *m/z* value before and after image fusion (Supplementary Figure 7). The ROC curve is composed of the sensitivity and (1-specificity) when using different intensity threshold to determine the status of the tissue. If the intensity of that *m/z* peak in the pixel is higher than the threshold, the pixel on the tissue is considered as cancer. Otherwise, the pixel will be assigned as normal. After that, the results were compared with H&E stained metastatic lung tissue image assigned by the pathologist to calculate the sensitivity and specificity of this ion. Ion with area under curve (AUC) of the ROC curve closer to one indicates greater potential to be a biomarker. The AUC value of 0.7 was used to determine whether the ion can represent cancerous region in a tissue section and be a potential biomarker. In Fig. 7a, *m/z* 749.4 had the AUC around 0.5, which showed that the distribution of the ion species was irrelevant to the status of the tissue. In contrast, *m/z* 743.4 had the AUC value higher than 0.7, which showed that there were good

correlations between DESI MSI and pathologist's interpretation. However, in the raw MSI, the distribution of the ions had obscure outlines and hard to differentiate the malignant tissue from normal tissue. Some potential biomarkers were neglected. In total, only 16 ions can be pick out as potential biomarkers. After image fusion, the outline of the ions was sharpened, making it easier for distinguishing between malignant and normal tissue. In Fig. 7b, the AUC of *m/z* 724.6 increased to higher than 0.7 after image fusion. This illustrated that this ion could be a potential biomarker, but the original image was blurred and was not suitable for cancer diagnosis. With higher resolution of MSI, an addition of 11 ion species can be determined as potential biomarkers. Some of these biomarkers were annotated basing on their MS/MS, and were shown in Supplementary Table 2.

We can easily diagnose the sites of malignant tissue sections with the aid of fine spatial resolution MSI. In-situ MS/MS analysis of several lipid species observed from the surface of breast tumor metastatic lung tissue using DESI is shown in Supplementary Table 2 (Tandem mass profiles shown in Supplementary Figure 9.). The distribution of these potential biomarkers had obscure outlines in the raw DESI MSI. The ambiguous outline throughout the cancer tissue was sharpened after image fusion, making it easier for distinguishing between the malignant and normal tissue. To further investigate the results, we compared the outcomes with standard pathology methods. In Fig. 6c and Fig. 6d, locations and margins of the cancerous cell of H&E stained tumor section were indicated and marked out by the pathologist.

**Discussion**

Ambient ionization has been widely studied and plenty of dedicated setups were built and reported for imaging directly from histological tissue sections for real-time analysis[10,16,18–21,49]. For ambient surface analysis, most of the methods are based on

liquid microjunction extraction targeting intact molecules such as liquid extraction surface analysis (LESA)[50,51], nanospray desorption electrospray ionization (nanoDESI)[7,10,11,18,20], Liquid microjunction surface sampling probe (LMJ/SSP)[52,53], whereas some techniques were based on laser ablation[54–57]. The pixel size of the images was determined by the area of the liquid junction size or the beam size of the laser beam. In order to reduce the size of the pixel, shrinking the diameter of the microjunction probe was another common strategy, but this approach limited the efficacy for in situ compound analysis due to the lower ion intensity and serious carryover effect caused by the decrement of solvent delivery rate and extraction efficiency[20,26]. Such drawbacks became the hindrance while performing higher spatial resolution imaging of ambient ionization. Sample ablation and analyte ionization by different types of laser sources integrated with electrospray ionization under atmospheric condition were also reported to be capable of generating fine resolution MSI[56,57]. The diameters of the ablated craters determined the pixel size of the images, which were typically between 200-400 μm, while pixel size of 20 μm was achieved with additional focus lens[57]. Recently, another laser ablation based mass spectrometry imaging technique were reported to accomplish mapping images with 2.9μm spatial resolution from special treated live tissue and with plasma ionization[33]. However, the *m/z* ranges these techniques were able to detect were limited. Introducing large molecules to the mass spectrometer was challenging due to the inefficient ion transportation and low ionization efficiency under ambient condition. Additionally, to acquire MSI at such a high spatial resolution, complex sample pretreatment and instrument remodeling were required in most approaches, which increase the manipulate difficulties and experimental expenditure.

In addition to the problem occur in instrumentation improvement or remodeling, long data acquisition time during analysis by high-resolution scanning may induce compound degradation. As the spatial resolution of MSI increases for an analysis,

scanning time increases as a square function. That is, when the spatial resolution of an MSI is doubled, analyze time consumption is quadrupled. Since the chemical composition of the sample can alter as the sample exposed to the environment, mitigating the analysis time is thus substantial[58]. On the other hand, as the spatial resolution of the MSI increases, the signal intensity decreases significantly. This issue limited the spatial resolution of the MSI, especially for ambient ionization methods, which have lower ion transportation efficiency. Utilizing numerical image fusion techniques allows dramatic increases not only in the spatial resolution of the MSI but also improves data throughput since intensive scanning is no longer required.

Matrix-assisted laser desorption ionization provides another avenue to analyze variant classes of molecules under vacuum environment and is capable of achieving subcellular spatial resolution. With modified instrument setup, molecules with *m/z* larger than 24 kDa was mapped out by the Fourier transform analyzer[59]. However, applying suitable matrix to assist the ionization of molecules would complex the sample pretreatment and could potentially perturb the localization of molecules during sample preparation. Moreover, strict conditions such as storing the samples under high vacuum system during analysis limited the flexibility of these techniques. AP-MALDI had been established to alleviate this shortcoming[60].However, the Ion loss in atmospheric pressure interfaces (API) and matrix interference at the low mass range remain as critical problems[61]. On the other hand, ambient ionization MSI methods provide simplified sample pretreatment and working condition, but often with coarse spatial resolution. Utilizing image fusion techniques to assemble rough MSI with optical microscopy was demonstrated as a solution to achieve higher spatial resolution. This approach could compensate the physical limitation (spraying cone region, liquid microjunction size… etc.) that most of the ambient ionization techniques face nowadays.

In conclusion, we showed that the image fusion of ambient ionization MSI with H&E staining microscopy image was able

to generate reliable images of molecular distribution in tissue. The fused images were validated by comparing with conventional MALDI MSI and IHC staining techniques. As minimum sample preparation and instrument adjustment is needed, image fusion of ambient ionization MSI with H&E staining images showed high potential in clinical diagnosis for cancer tissue sections. We believe that our results could provide a contribution towards this end.

**Methods**

**Application of image fusion on ambient ionization MSI.** We demonstrated the integration of optical microscopy with ambient ionization MSI using image fusion to obtain high spatial resolution MSI. In our study, serial mouse brain and kidney tissue sections were chosen for performing MSI techniques based on their complex morphology and enriched chemicals on different regions of the sections. An illustration of the workflow of experiment procedure is shown in Fig. 7, raw files of mass spectra of tissue sections were converted into 2D ion images after data collection from DESI and nanoDESI analysis, while H&E residual sections (in DESI) and adjacent sections (in nanoDESI) photographs were taken using an optical microscope. The retrieved images were then imported into the software package for chemically spatial distributable prediction of peaks of interested and generated the results. Ambient ionization source experimental setups was shown in Supplementary Figure 1 and introduction of image fusing procedures was briefly described in Supplementary Figure 3.

**Desorption electrospray ionization.** For DESI images, commercial DESI source was mounted to Orbitrap Elite to conduct the experiment. The gas pressure of nitrogen was set at 150 psi, the angle of the spray head was set to 55˚, the flow rate of the solvent (DMF:ACN = 1:1) was 2 μl/min and the voltage was 3.5 kV.

**Nanospray desorption electrospray ionization.** The nanoDESI system is based on commercial DESI platform, two flame-pulled fused

capillaries (O.D: 360μm, I.D: 250μm) were implanted and used to substitute the original DESI emitter as the ion source. The solvent delivery (primary) capillary (65% ACN with 1% formic acid), is applied with a high voltage (2.5kV) to extract and ionize the compound on the surface of the sample. The secondary capillary was used to deliver the extracts from the sample to the mass spectrometer by creating nanospray.

**Tissue samples.** Mice brain and kidney tissues were bought from BioLASCO Taiwan Co., Ltd. Gender and age of the ICR mice were not specified. Lung tissues containing metastatic tumors from a breast cancer mice model were gifts from Dr. Tang-Long Shen's lab in National Taiwan University. These mice were handled in accordance with a protocol approved by the Institutional Animal Care and Use Committee of National Taiwan University (IACUC approval NO. NTU104-EL-00003). The intact organs were harvested as soon as euthanasia and then stored under -80˚C prior cryo-sectioning. For tissue cryo-sectioning, organs were flash-frozen using liquid nitrogen and kept under -20˚C in the cold tome (LEICA, CM1900) in order to reach the suitable temperature before sectioning. Tissue samples were sectioned to 14-μm thick sections and thaw-mounted onto the slides and stored at -80˚C prior to analysis without fixation. Slides used for nanoDESI analysis were regular plain glass without any coating. For DESI, H&E staining and immunostaining, tissues were thaw-mounted onto silane coated slides; while the slides for MALDI analysis were indium tin oxide coated. Before nanoDESI MS interrogation, tissue sections were dried in a dissector for ~1 hour and then deep into 50 ml chloroform and rinsed for 1 min. Adjoining tissue section pretreatment for MALDI validation is mentioned in the following. The matrix application was achieved by sublimation method, which was described elsewhere[62], followed by a recrystallization step[63]. The sublimation apparatus was purchased from Singlong (Taichung, Taiwan). The apparatus was placed in a sand bath on a hot plate while applying matrix. The brain sections were adhered to ITO-coated glass slides by a conductive tape and stored under -80°C before applying matrix. Sublimation was performed using 2,5-dihydroxyacetophenone (2,5-DHA). The matrix sublimation and application were performed at 110 °C with a 0.7 Torr vacuum for 10 minutes. Amount of the applied matrices were determined by the exposure time. The matrix-coated samples were

rehydrated with 50% TFA solution in an incubator at 37 °C for 4 minutes. A sonication step was added to increase the signal for protein analysis[64]. The sonication was operated by Elmasonic S 30 H ultrasonicator under continuous mode with frequency of 37 KHz. As for DESI MS interrogation, tissue sections were dried in a dissector for ~1 hour, no further sample pretreatment is required before analysis**.**

**H&E staining.** The residual tissue slides scanned by DESI or nanoDESI and their adjoining tissue slides were rinsed with 70% EtOH and then 100% EtOH for 30s each and allow dry under vacuum. The hematoxylin staining was applied under 60˚C for 40s. After hematoxylin staining, the slides were rinsed with $H_2O$, then rinsed with acidified EtOH 0.3% for 3s, then rinsed with $H_2O$. The blueing up was achieved by 1%$NH_4OH$ and finally $H_2O$ under room temperature. Then the slides were dipped into the eosin stain for 20s, then the slides were rinsed with $H_2O$, then 80%EtOH, then 90%EtOH, and finally 99% EtOH at room temperature.

**Top-Down Protein Analysis.** Protein ions were directly introduced to the LTQ Orbitrap Elite using the same platform for tandem mass analysis, protein of interest was chosen as the mass center of 5 *m/z* isolation window with an activation energy Q of 0.25 and utilize collision energy of 30%. The data was imported into Prosight PTM for identification[65,66].

**High performance liquid chromatography–mass spectrometry.** Brain tissue was extracted with MTBE methods[67]. The HPLC-MS/MS analysis was performed using HPLC (LC-20AD, Shimadzu, Tokyo, Japan), coupled with Orbitrap Elite (Thermo Scientific). HPLC experiments were performed using C18 column (100*2.1mm, 3.5µm, Agilent) and following the gradient elution: mobile phase A= water with 0.1% formic acid (v/v); mobile phase B= acetonitrile and isopropanol (10:90, v/v) with 0.1 % formic acid (v/v); elution profile= 0.0-5.0 min (40% mobile phase B); 5.0-35.0 min (40-90% mobile phase B); 35.0-50.0 min (90% mobile phase B), column oven at 25°C, volume injection 10 µL and flow rate of 0.15 mL/min. Mass spectrometry acquisition parameters were as followed: positive ions mode, heater temperature 180°C, sheath gas flow rate 35 arb, auxiliary gas flow rate 10 arb, sweep gas flow rate 10 arb, spray voltage 3.5 kV and capillary temperature 350°C. CID fragmentation

was performed for targeting ion peaks observed in DESI analysis with collision energy of 30% and an activation Q of 0.25. The MS spectra were collected in FT mode with 30,000 resolving power. The mass spectral analysis was processed by Xcalibur QualBrowser.

**Immunofluorescence staining.** All the procedures for immunostaining are based on the description of the commercial kit (TAHC03, BioTnA, Kaohsiung, Taiwan). After immunostaining, the slides were mounted and digitized with an Motic Easyscan Digital Slide Scanner (Motic Hong Kong Limited, Hong Kong, China) at ×40 (0.26 μm/pixel) with high precision (High precision autofocus). Motic Easyscan whole-slide images were viewed with DSAssistant and EasyScanner software at Litzung Biotechnology INC (Kaohsiung, Taiwan).

**Matrix-assisted laser desorption/ionization.** MALDI mass spectrometry images were acquired using MALDI-TOF/TOF mass spectrometry (Autoflex Speed MALDI TOF/TOF system, Bruker Daltonics). The instrument was equipped with the third harmonic of Nd:YAG SmartBeamTM-II laser (355nm). Imaging spectra were recorded and processed by flexControl 3.4 and flexImaging 3.0 (Bruker Daltonics). The spectra were acquired in positive polarity with pixel-to-pixel resolution of 60μm using the following parameters: laser attenuator offset at 80% of the maximum power; laser operating power at 90% under linear mode for protein analysis and 80% under reflectron mode for lipid analysis with smartbeam parameter at 2_small; laser repetition rate at 1 kHz; acquisition shots accumulated to 1,000 shots per pixel for imaging analysis. The resulting imaging spectra were processed using TopHat baseline subtraction and normalized to the total ion counts per pixel.

**MSI data acquisition.** The experiments were conducted using Prosolia's commercial DESI 2D system. The scanning rate of the motor stage for nanoDESI and DESI was approximate 30μm $s^{-1}$ and 150μm $s^{-1}$, respectively. The acquisition raw data were then import into Firefly$^{TM}$ 2.2 data conversion software for data conversion, then we imported the converted data into BioMAP to obtain the final DESI and nanoDESI image.

**Image fusion data pretreatment.** The MSI data was converted into .img file by Firefly$^{TM}$ 2.2 and exported into a built-in matlab package MSiReader. The region of interest for each datasets was determined empirically by overlapping the H&E image and the MSI data in

MSiReader[68]. The signals were binned into 2,000 bins and summed before exported as uniformly spaced text file. The microscope images were collected by an optical microscope (WHITED INC., Taipei, Taiwan) with a PSC600-05C digital camera (OPLENIC CORP., USA) and data processed by AOR AJ-VERT. The microscopy images were then exported as a uniform data array by in-house generated Matlab script. An affine transform matrix that can describe the spatial relationship between MSI data and microscopy data was calculated using an in-house generated script. The alignment of the data sets was done by aligning upsampled MSI data and the microscopic data to ensure the best fitting. In detail, three pixels in the MSI were selected for the teaching point setting. The image of the MSI was interpolated by dividing each pixel into 36 smaller sub-pixels (6*6 sub-pixels per original pixel) and the four sub-pixels at the center were colored. The upsampled MSI data was aligned with the microscopic image manually by adjusting the transparency of both images. The teaching points on the microscopy image were determined by the center of the colored sub-pixels on the upsampled MSI image.

The processed data was exported by in-house generated Matlab script and imported into “Molecular image fusion system” under command-line interface.

**Data and code availability.** The mass spectrum for MS/MS annotations are included in the Supplementary information. Other materials and MATLAB code are available from the corresponding author upon reasonable request.

**References**


1. Pohl, C. & Genderen, J. L. V. Review article Multisensor image fusion in remote sensing: Concepts, methods and applications. *Int. J. Remote Sens.* **19**, 823–854 (1998).

2. Xydeas, C. S. & Petrovic, V. Objective image fusion performance measure. *Electron. Lett.* **36**, 308–309 (2000).

3. Li, H., Manjunath, B. S. & Mitra, S. K. Multisensor Image Fusion Using the Wavelet Transform. *Graph. Models Image Process.* **57**, 235–245 (1995).

4. James, A. P. & Dasarathy, B. V. Medical image fusion: A survey of the state of the art. *Inf. Fusion* **19**, 4–19 (2014).

5. Ma, J., Ma, Y. & Li, C. Infrared and visible image fusion methods and applications: A survey. *Inf. Fusion* **45**, 153–178 (2019).

6. Ghassemian, H. A review of remote sensing image fusion methods. *Inf. Fusion* **32**, 75–89 (2016).

7. Khatib-Shahidi, S., Andersson, M., Herman, J. L., Gillespie, T. A. & Caprioli, R. M. Direct Molecular Analysis of Whole-Body Animal Tissue Sections by Imaging MALDI Mass Spectrometry. *Anal. Chem.* **78**, 6448–6456 (2006).

8. Wiseman, J. M. *et al.* Desorption electrospray ionization mass spectrometry: Imaging drugs and metabolites in tissues. *Proc. Natl. Acad. Sci. U. S. A.* **105**, 18120–18125 (2008).

9. Trim, P. J. *et al.* Matrix-Assisted Laser Desorption/Ionization-Ion Mobility Separation-Mass Spectrometry Imaging of Vinblastine in Whole Body Tissue Sections. *Anal. Chem.* **80**, 8628–8634 (2008).

10. Hsu, C.-C. & Dorrestein, P. C. Visualizing life with ambient mass spectrometry. *Curr. Opin. Biotechnol.* **31**, 24–34 (2015).

11. Hsu, C.-C., Chou, P.-T. & Zare, R. N. Imaging of Proteins in Tissue Samples Using Nanospray Desorption Electrospray

Ionization Mass Spectrometry. *Anal. Chem.* **87**, 11171–11175 (2015).

12. Gouw, A. M. *et al.* Oncogene KRAS activates fatty acid synthase, resulting in specific ERK and lipid signatures associated with lung adenocarcinoma. *Proc. Natl. Acad. Sci.* **114**, 4300–4305 (2017).

13. Ifa, D. R. & Eberlin, L. S. Ambient Ionization Mass Spectrometry for Cancer Diagnosis and Surgical Margin Evaluation. *Clin. Chem.* **62**, 111–123 (2016).

14. Sans, M., Feider, C. L. & Eberlin, L. S. Advances in mass spectrometry imaging coupled to ion mobility spectrometry for enhanced imaging of biological tissues. *Curr. Opin. Chem. Biol.* **42**, 138–146 (2018).

15. Zhang, J. *et al.* Cardiolipins Are Biomarkers of Mitochondria-Rich Thyroid Oncocytic Tumors. *Cancer Res.* **76**, 6588–6597 (2016).

16. Takáts, Z., Wiseman, J. M., Gologan, B. & Cooks, R. G. Mass Spectrometry Sampling Under Ambient Conditions with Desorption Electrospray Ionization. *Science* **306**, 471–473 (2004).

17. Hsu, C.-C. *et al.* Real-time metabolomics on living microorganisms using ambient electrospray ionization flow-probe. *Anal. Chem.* **85**, 7014–7018 (2013).

18. Roach, P. J., Laskin, J. & Laskin, A. Nanospray desorption electrospray ionization: an ambient method for liquid-extraction surface sampling in mass spectrometry. *Analyst* **135**, 2233–2236 (2010).

19. Lane, A. *et al.* Desorption electrospray ionization mass spectrometry reveals surface-mediated antifungal chemical defense of a tropical seaweed. *Proc. Natl. Acad. Sci. U. S. A.* **106**, 7314–9 (2009).

20. Laskin, J., Heath, B. S., Roach, P. J., Cazares, L. & Semmes, O. J. Tissue Imaging Using Nanospray Desorption Electrospray

Ionization Mass Spectrometry. *Anal. Chem.* **84**, 141–148 (2012).

21. Kauppila, T. J. *et al.* Desorption electrospray ionization mass spectrometry for the analysis of pharmaceuticals and metabolites. *Rapid Commun. Mass Spectrom. RCM* **20**, 387–392 (2006).

22. Takáts, Z., Wiseman, J. M. & Cooks, R. G. Ambient mass spectrometry using desorption electrospray ionization (DESI): instrumentation, mechanisms and applications in forensics, chemistry, and biology. *J. Mass Spectrom.* **40**, 1261–1275 (2005).

23. Banerjee, S. *et al.* Diagnosis of prostate cancer by desorption electrospray ionization mass spectrometric imaging of small metabolites and lipids. *Proc. Natl. Acad. Sci. U. S. A.* **114**, 3334–3339 (2017).

24. Eberlin, L. S. *et al.* Classifying Human Brain Tumors by Lipid Imaging with Mass Spectrometry. *Cancer Res.* **72**, 645–654 (2012).

25. Zhang, J. *et al.* Nondestructive tissue analysis for ex vivo and in vivo cancer diagnosis using a handheld mass spectrometry system. *Sci. Transl. Med.* **9**, eaan3968 (2017).

26. McDonnell, L. A. *et al.* Peptide and protein imaging mass spectrometry in cancer research. *J. Proteomics* **73**, 1921–1944 (2010).

27. Schwamborn, K. & Caprioli, R. M. Molecular imaging by mass spectrometry — looking beyond classical histology. *Nat. Rev. Cancer* **10**, 639–646 (2010).

28. Rao, W., Pan, N., Tian, X. & Yang, Z. High-Resolution Ambient MS Imaging of Negative Ions in Positive Ion Mode: Using Dicationic Reagents with the Single-Probe. *J. Am. Soc. Mass Spectrom.* **27**, 124–134 (2016).

29. Rae Buchberger, A., DeLaney, K., Johnson, J. & Li, L. Mass Spectrometry Imaging: A Review of Emerging Advancements and

Future Insights. *Anal. Chem.* **90**, 240–265 (2018).

30. Cooks, R. G., Ouyang, Z., Takats, Z. & Wiseman, J. M. Ambient Mass Spectrometry. *Science* **311**, 1566–1570 (2006).

31. McDonnell, L. A. & Heeren, R. M. A. Imaging mass spectrometry. *Mass Spectrom. Rev.* **26**, 606–643 (2007).

32. Ovchinnikova, O. S., Kjoller, K., Hurst, G. B., Pelletier, D. A. & Van Berkel, G. J. Atomic Force Microscope Controlled Topographical Imaging and Proximal Probe Thermal Desorption/Ionization Mass Spectrometry Imaging. *Anal. Chem.* **86**, 1083–1090 (2014).

33. Kim, J. Y. *et al.* Atmospheric pressure mass spectrometric imaging of live hippocampal tissue slices with subcellular spatial resolution. *Nat. Commun.* **8**, 2113 (2017).

34. Lee, J. K., Jansson, E. T., Nam, H. G. & Zare, R. N. High-Resolution Live-Cell Imaging and Analysis by Laser Desorption/Ionization Droplet Delivery Mass Spectrometry. *Anal. Chem.* **88**, 5453–5461 (2016).

35. Kertesz, V. & Van Berkel, G. J. Improved imaging resolution in desorption electrospray ionization mass spectrometry. *Rapid Commun. Mass Spectrom. RCM* **22**, 2639–2644 (2008).

36. Van de Plas, R., Yang, J., Spraggins, J. & Caprioli, R. M. Image fusion of mass spectrometry and microscopy: a multimodality paradigm for molecular tissue mapping. *Nat. Methods* **12**, 366–372 (2015).

37. Neumann, E. K. *et al.* Multimodal Chemical Analysis of the Brain by High Mass Resolution Mass Spectrometry and Infrared Spectroscopic Imaging. *Anal. Chem.* **90**, 11572–11580 (2018).

38. Vollnhals, F. *et al.* Correlative Microscopy Combining Secondary Ion Mass Spectrometry and Electron Microscopy: Comparison of Intensity–Hue–Saturation and Laplacian Pyramid Methods for Image Fusion. *Anal. Chem.* **89**, 10702–10710

(2017).

39. Jarmusch, A. K. *et al.* Differential Lipid Profiles of Normal Human Brain Matter and Gliomas by Positive and Negative Mode Desorption Electrospray Ionization – Mass Spectrometry Imaging. *PLOS ONE* **11**, e0163180 (2016).

40. Martínez-Gardeazabal, J. *et al.* Lipid mapping of the rat brain for models of disease. *Biochim. Biophys. Acta BBA - Biomembr.* **1859**, 1548–1557 (2017).

41. Vidová, V. *et al.* Laser Desorption-Ionization of Lipid Transfers: Tissue Mass Spectrometry Imaging without MALDI Matrix. *Anal. Chem.* **82**, 4994–4997 (2010).

42. Römpp, A., Guenther, S., Takats, Z. & Spengler, B. Mass spectrometry imaging with high resolution in mass and space (HR2 MSI) for reliable investigation of drug compound distributions on the cellular level. *Anal. Bioanal. Chem.* **401**, 65–73 (2011).

43. Hsu, C.-C. *et al.* Top-Down Atmospheric Ionization Mass Spectrometry Microscopy Combined With Proteogenomics. *Anal. Chem.* **89**, 8251–8258 (2017).

44. Ramos-Vara, J. A. & Miller, M. A. When Tissue Antigens and Antibodies Get Along: Revisiting the Technical Aspects of Immunohistochemistry—The Red, Brown, and Blue Technique. *Vet. Pathol.* **51**, 42–87 (2014).

45. Diamandis, E. P. Mass Spectrometry as a Diagnostic and a Cancer Biomarker Discovery Tool: Opportunities and Potential Limitations. *Mol. Cell. Proteomics* **3**, 367–378 (2004).

46. Eberlin, L. S. *et al.* Molecular assessment of surgical-resection margins of gastric cancer by mass-spectrometric imaging. *Proc. Natl. Acad. Sci. U. S. A.* **111**, 2436–2441 (2014).

47. Zhang, J. *et al.* Detection of Metastatic Breast and Thyroid Cancer in Lymph Nodes by Desorption Electrospray Ionization

Mass Spectrometry Imaging. *J. Am. Soc. Mass Spectrom.* **28**, (2017).

48. Lopez-Garcia, M. A., Geyer, F. C., Lacroix-Triki, M., Marchió, C. & Reis-Filho, J. S. Breast cancer precursors revisited: molecular features and progression pathways. *Histopathology* **57**, 171–192 (2010).

49. Laskin, J. & Lanekoff, I. Ambient Mass Spectrometry Imaging Using Direct Liquid Extraction Techniques. *Anal. Chem.* **88**, 52–73 (2016).

50. Kertesz, V. & Berkel, G. J. V. Fully automated liquid extraction-based surface sampling and ionization using a chip-based robotic nanoelectrospray platform. *J. Mass Spectrom.* **45**, 252–260 (2010).

51. Eikel, D. *et al.* Liquid extraction surface analysis mass spectrometry (LESA-MS) as a novel profiling tool for drug distribution and metabolism analysis: the terfenadine example. *Rapid Commun. Mass Spectrom.* **25**, 3587–3596 (2011).

52. Van Berkel, G. J., Sanchez, A. D. & Quirke, J. M. E. Thin-Layer Chromatography and Electrospray Mass Spectrometry Coupled Using a Surface Sampling Probe. *Anal. Chem.* **74**, 6216–6223 (2002).

53. Kertesz, V., Ford, M. J. & Van Berkel, G. J. Automation of a Surface Sampling Probe/Electrospray Mass Spectrometry System. *Anal. Chem.* **77**, 7183–7189 (2005).

54. Ovchinnikova, O. S., Bhandari, D., Lorenz, M. & Van Berkel, G. J. Transmission geometry laser ablation into a non-contact liquid vortex capture probe for mass spectrometry imaging. *Rapid Commun. Mass Spectrom.* **28**, 1665–1673 (2014).

55. Ovchinnikova, O. S., Kertesz, V. & Van Berkel, G. J. Combining Laser Ablation/Liquid Phase Collection Surface Sampling and High-Performance Liquid Chromatography−Electrospray Ionization-Mass Spectrometry. *Anal. Chem.* **83**, 1874–1878 (2011).

56. Nemes, P. & Vertes, A. Laser Ablation Electrospray Ionization for Atmospheric Pressure, in Vivo, and Imaging Mass Spectrometry. *Anal. Chem.* **79**, 8098–8106 (2007).

57. Shelley, J. T., Ray, S. J. & Hieftje, G. M. Laser Ablation Coupled to a Flowing Atmospheric Pressure Afterglow for Ambient Mass Spectral Imaging. *Anal. Chem.* **80**, 8308–8313 (2008).

58. Prentice, B. M. & Caprioli, R. M. The Need for Speed in Matrix-Assisted Laser Desorption/Ionization Imaging Mass Spectrometry. *Postdoc J. J. Postdr. Res. Postdr. Aff.* **4**, 3–13 (2016).

59. Prentice, B. M., Ryan, D. J., Van de Plas, R., Caprioli, R. M. & Spraggins, J. M. Enhanced Ion Transmission Efficiency up to m/z 24 000 for MALDI Protein Imaging Mass Spectrometry. *Anal. Chem.* **90**, 5090–5099 (2018).

60. Laiko, V. V., Baldwin, M. A. & Burlingame, A. L. Atmospheric Pressure Matrix-Assisted Laser Desorption/Ionization Mass Spectrometry. *Anal. Chem.* **72**, 652–657 (2000).

61. Laiko, V. V., Moyer, S. C. & Cotter, R. J. Atmospheric Pressure MALDI/Ion Trap Mass Spectrometry. *Anal. Chem.* **72**, 5239–5243 (2000).

62. Hankin, J. A., Barkley, R. M. & Murphy, R. C. Sublimation as a Method of Matrix Application for Mass Spectrometric Imaging. *J. Am. Soc. Mass Spectrom.* **18**, 1646–1652 (2007).

63. Yang, J. & Caprioli, R. M. Matrix Sublimation/Recrystallization for Imaging Proteins by Mass Spectrometry at High Spatial Resolution. *Anal. Chem.* **83**, 5728–5734 (2011).

64. Lin, L.-E., Su, P.-R., Wu, H.-Y. & Hsu, C.-C. A Simple Sonication Improves Protein Signal in Matrix-Assisted Laser Desorption Ionization Imaging. *J. Am. Soc. Mass Spectrom.* **29**, 796–799 (2018).

65. LeDuc, R. D. & Kelleher, N. L. Using ProSight PTM and Related Tools for Targeted Protein Identification and Characterization with High Mass Accuracy Tandem MS Data. *Curr. Protoc. Bioinforma.* **19**, 13.6.1-13.6.28 (2007).

66. Zamdborg, L. *et al.* ProSight PTM 2.0: improved protein identification and characterization for top down mass spectrometry. *Nucleic Acids Res.* **35**, W701-706 (2007).

67. Matyash, V., Liebisch, G., Kurzchalia, T. V., Shevchenko, A. & Schwudke, D. Lipid extraction by methyl-tert-butyl ether for high-throughput lipidomics. *J. Lipid Res.* **49**, 1137–1146 (2008).

68. Robichaud, G., Garrard, K. P., Barry, J. A. & Muddiman, D. C. MSiReader: an open-source interface to view and analyze high resolving power MS imaging files on Matlab platform. *J. Am. Soc. Mass Spectrom.* **24**, 718–721 (2013).

## Additional information


### Acknowledgments

We acknowledge the laboratory technique service of histology and pathology at Litzung Biotechnology INC., Kaohsiung, Taiwan. All tissue sections were analyzed and scored by the experienced veterinary pathologist, Hao-Kai,Chang (Litzung Biotechnology INC., Kaohsiung, Taiwan; BioTnA, Kaohsiung, Taiwan). Li-En Lin was supported by MOST grant 106-2813-C-002-136-M.


### Author Contributions

C.L.C., L.E.L., Y.C.H. and H.H.C. conducted experiments; C.L.C., L.E.L. and H.H.C. performed data processing; C.L.C., L.E.L. and C.C.H. conceived and designed the research; C.L.C., L.E.L. and C.C.H. wrote the article. All authors have read and approved the final manuscript.

### Competing interests

The authors declare no competing financial interests.

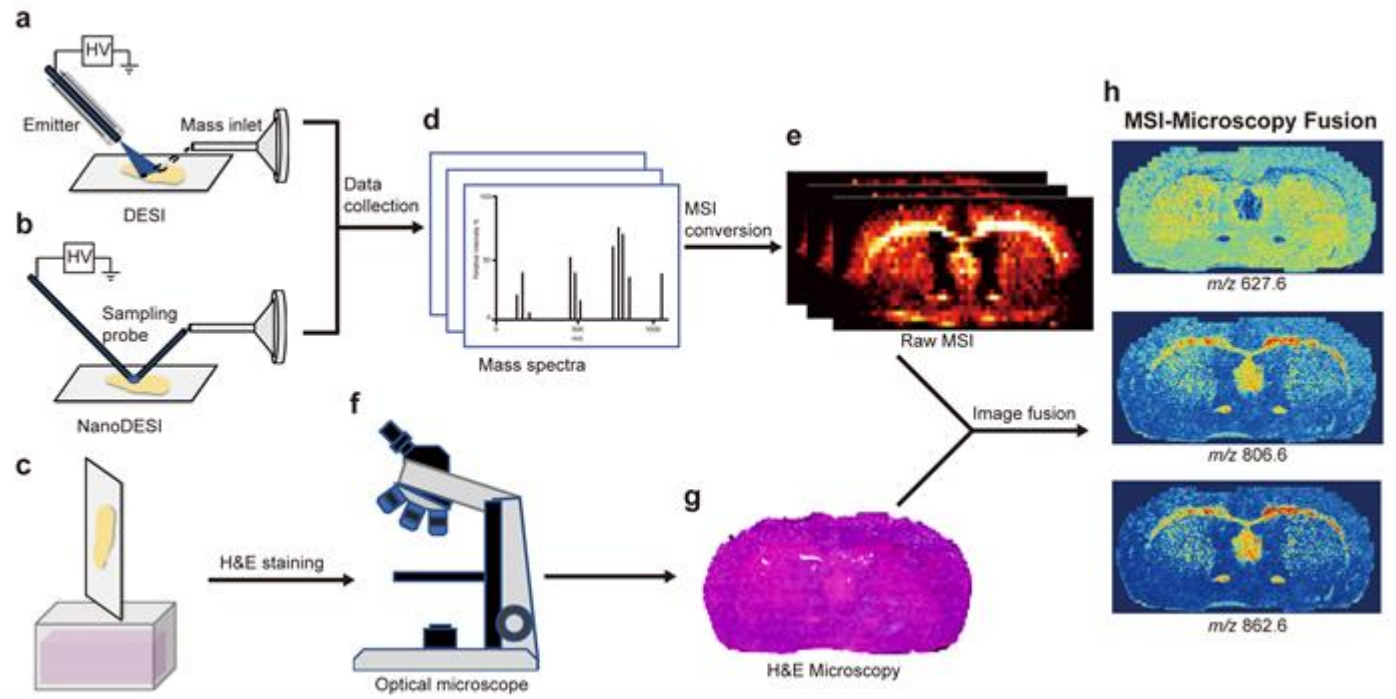


**Fig. 1** Illustration of the ambient ionization data acquisition and mass spectra image fusion process. (a) Scheme of desorption electrospray ionization setup. (b) Homemade nanospray desorption electrospray ionization source. (c), (f), (g) H&E stained serial sections microscopy image acquisition procedure. (d) MS data collection from ambient ionization sources. (e) Peak based serial MS images. After MSI data collection from the ambient ionization sources, optical microscopies of H&E stained residue (for DESI) or adjacent (for nanoDESI) sections were employed for chemical spatial distribution prediction based on statistic measurement to profile higher spatial resolution molecular distributions.

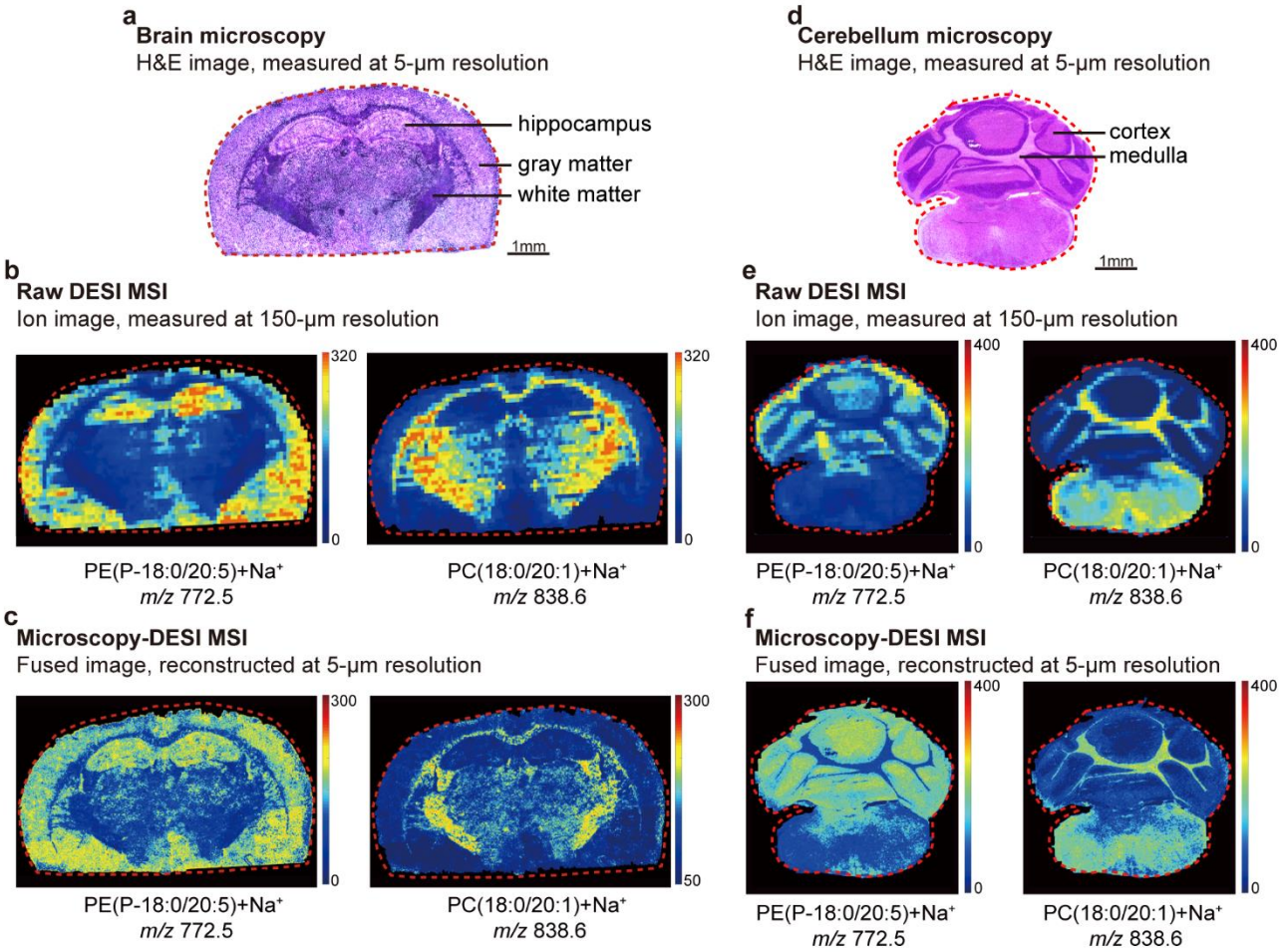


**Fig. 2** Lipid distribution of brain and cerebellum mapped by DESI MSI. (a) H&E stained brain section. (b) Raw DESI-MSI of lipid species. (c) Predicted high spatial resolution MSI after applying mage fusion. (d) H&E stained cerebellum section. (e) Raw DESI-MSI of lipid species. (f) Predicted high spatial resolution MSI after applying image fusion. Small molecules such as lipid were ionized using DESI and carried to the mass spectrometry by secondary droplets.

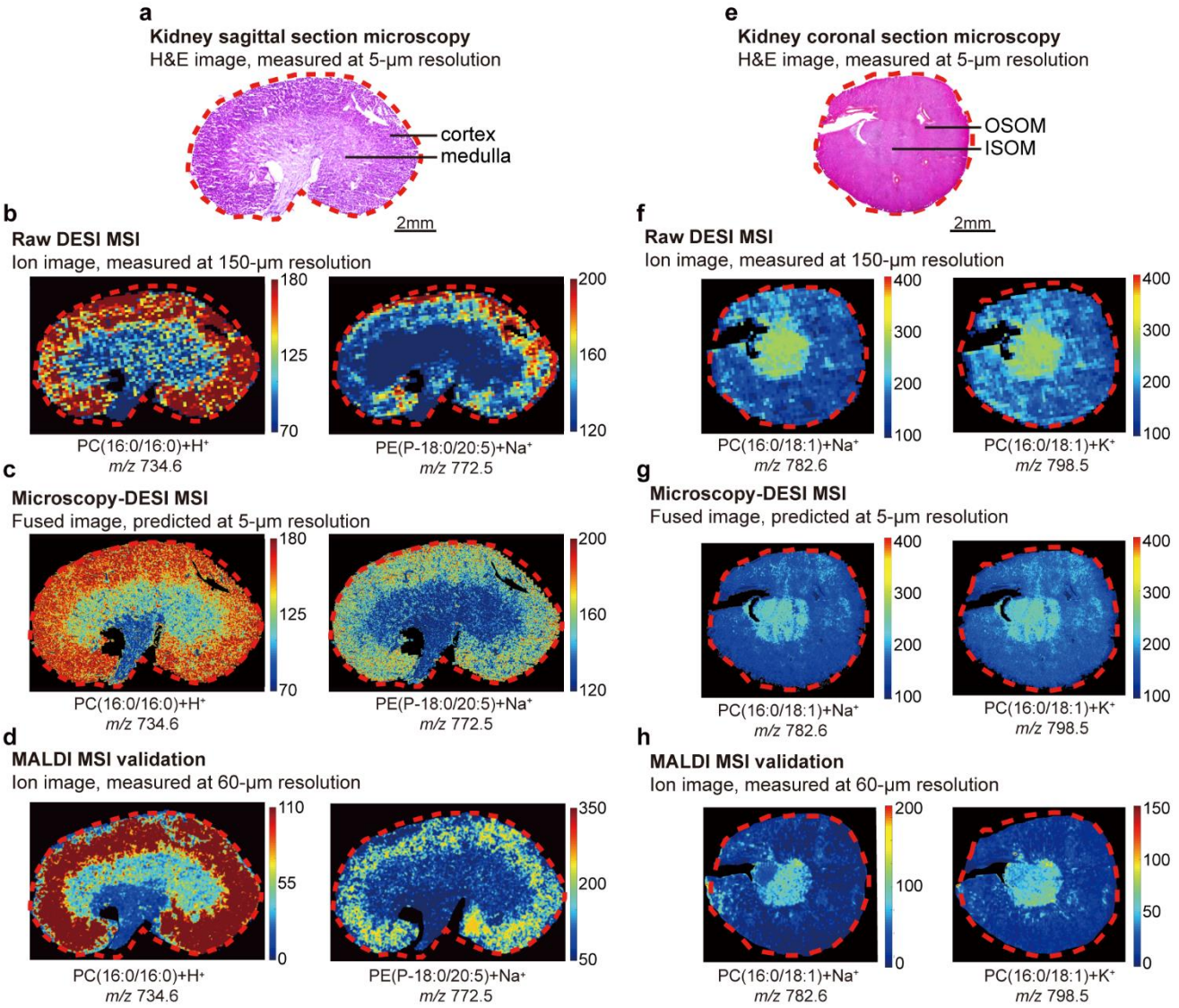


**Fig. 3** Lipid distribution of kidney sagittal and coronal sections by DESI and MALDI analysis. (a) Sagittal section of mouse kidney. (b) Raw DESI MSI visualized lipid protonated and sodium adducts of PC (16:0/16:0) and PE(P-18:0/20:5), respectively. (c) Predicted high spatial resolution MSI after applying image fusion. (d) Adjoining sections of kidney sagittal sections mapped by MALDI MSI for distribution of lipid species. (e) Coronal section of mouse kidney. (f) Raw DESI MSI visualized same lipid PC (16:0/18:1) sodium and potassium adducts local distribution, respectively. (g) Predicted high spatial resolution MSI after applying image fusion. (h) Adjoining sections of kidney coronal sections mapped by MALDI MSI for distribution of lipid species.

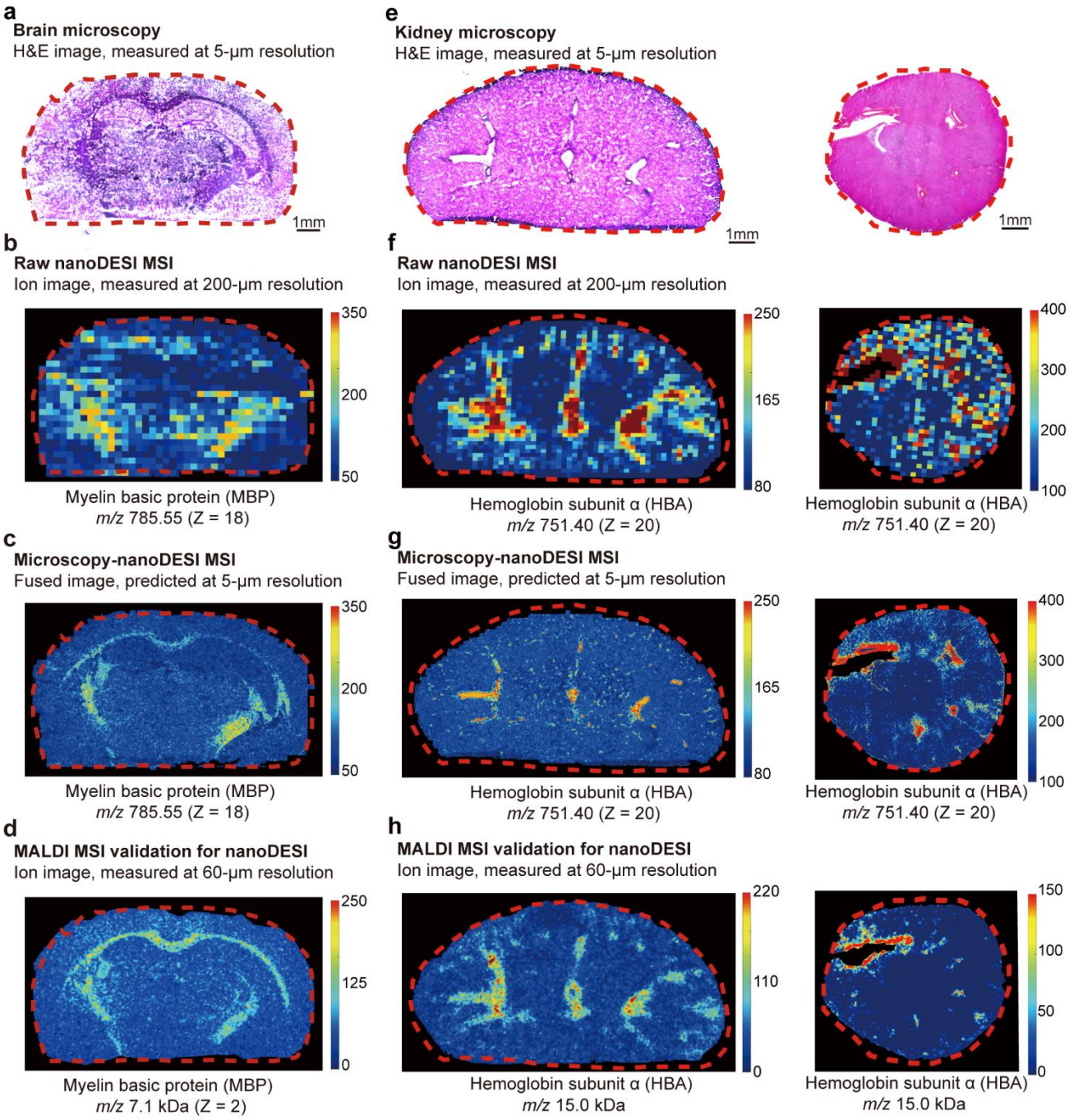


**Fig. 4** Protein distribution of brain and kidney sections by nanoDESI and MALDI analysis. (a) H&E stained adjacent brain tissue of nanoDESI analysis. (b) Raw DESI MSI visualized MBP at 200 μm spatial resolution. (c) Predicted high spatial resolution molecular distribution of MBP after applying image fusion. (d) Adjoining sections of brain sections mapped by MALDI MSI for distribution of MBP. (e) H&E stained adjacent kidney tissue of nanoDESI analysis. (f) Raw nanoDESI MSI visualized HBA at 200 μm spatial resolution. (g) Predicted high spatial resolution molecular distribution of HBA after applying image fusion. (h) Adjoining sections of kidney sections mapped by MALDI MSI for distribution of HBA.

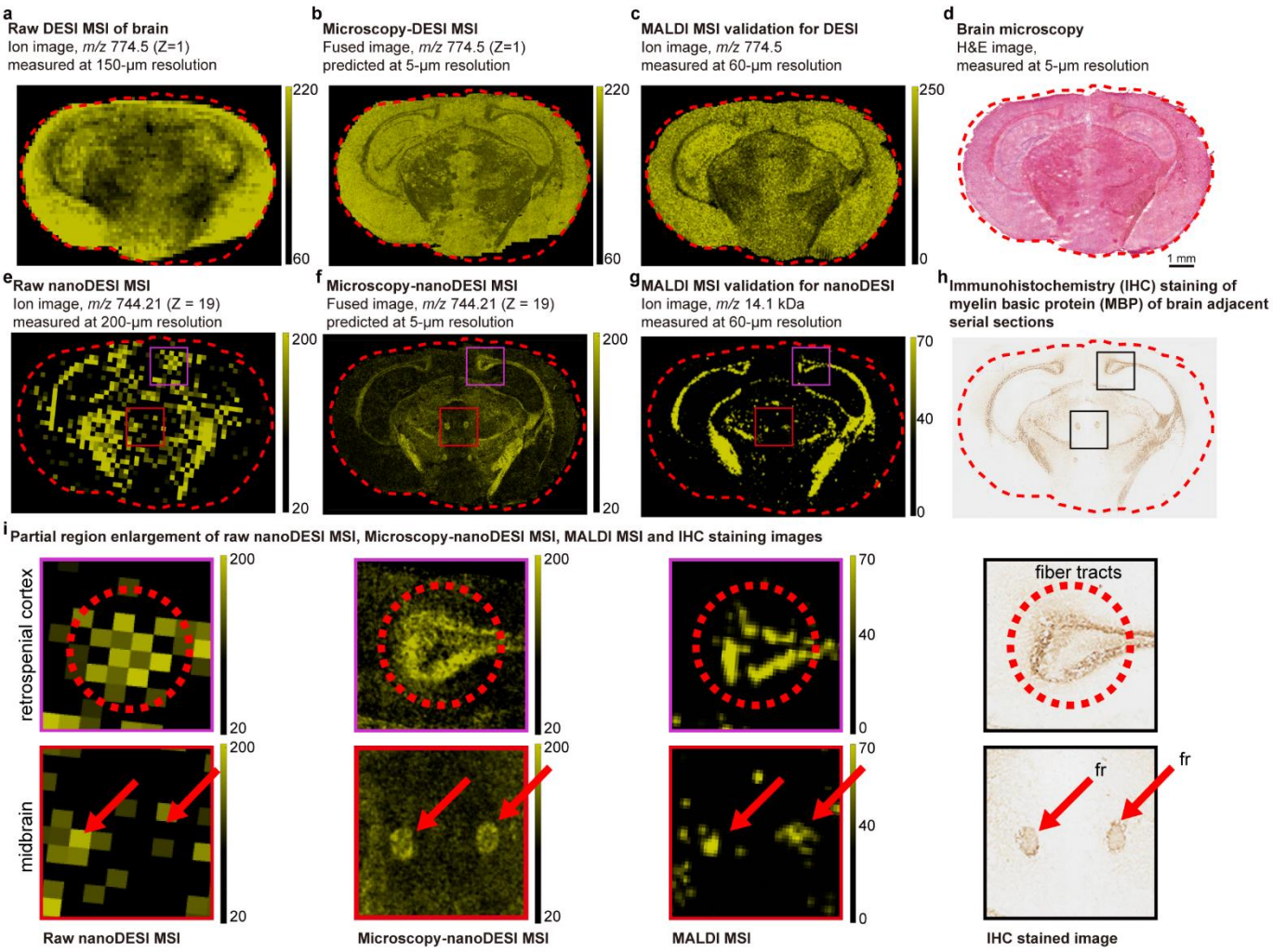


**Fig. 5** Brain serial section of DESI, nanoDESI, MALDI and immunohistochemistry mapping. (a) Raw DESI MSI analysis of lipid species. (b) Predicted high spatial resolution MSI of DESI analysis after applying image fusion. (d) Ion distribution validation by MALDI analysis. (d) H&E stained serial section. (e) Raw nanoDESI MSI analysis of myelin basic protein. (f) Predicted high spatial resolution MSI of nanoDESI analysis after applying image fusion. (g) Ion distribution validation by MALDI analysis. (h) Immunohistochemistry (IHC) staining of myelin basic protein. (i) Enlarged images of raw nanoDESI MSI, MSI-microscopy image, MALDI MSI and IHC staining.

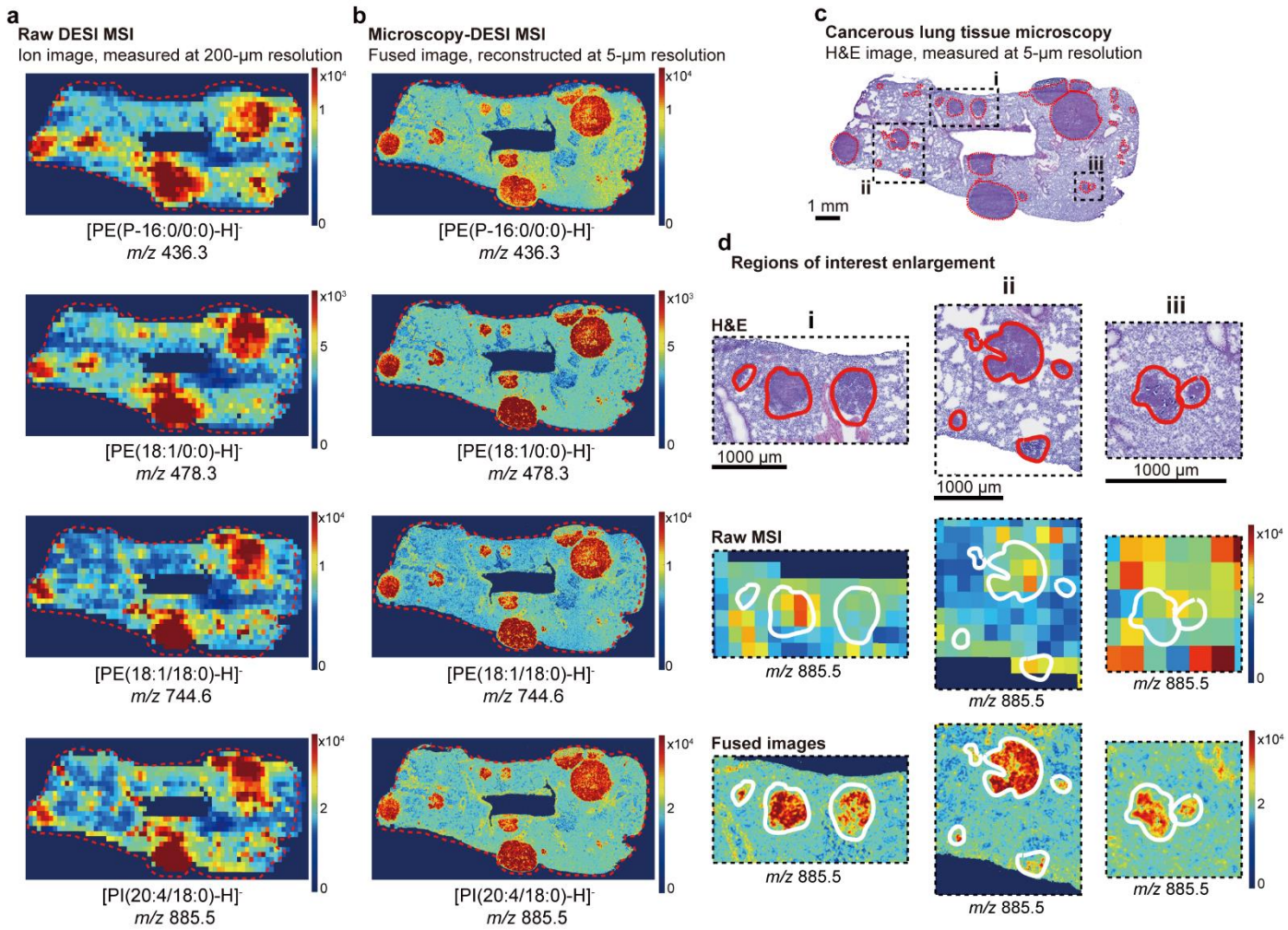


**Fig. 6** Cancerous lung tissue section analysis. DESI MSI was conducted under negative mode for depicting lipids species of the metastatic breast cancer tissue section of mouse lung. (a) Raw DESI-MSI of lipid species. (b) Predicted high spatial resolution MSI after applying image fusion. (c) H&E stained lung tissue section. (d) Enlarged images of microscopy image, raw DESI MSI and MSI-microscopy image of [PI(20:4/18:0)-H]$^-$ species.

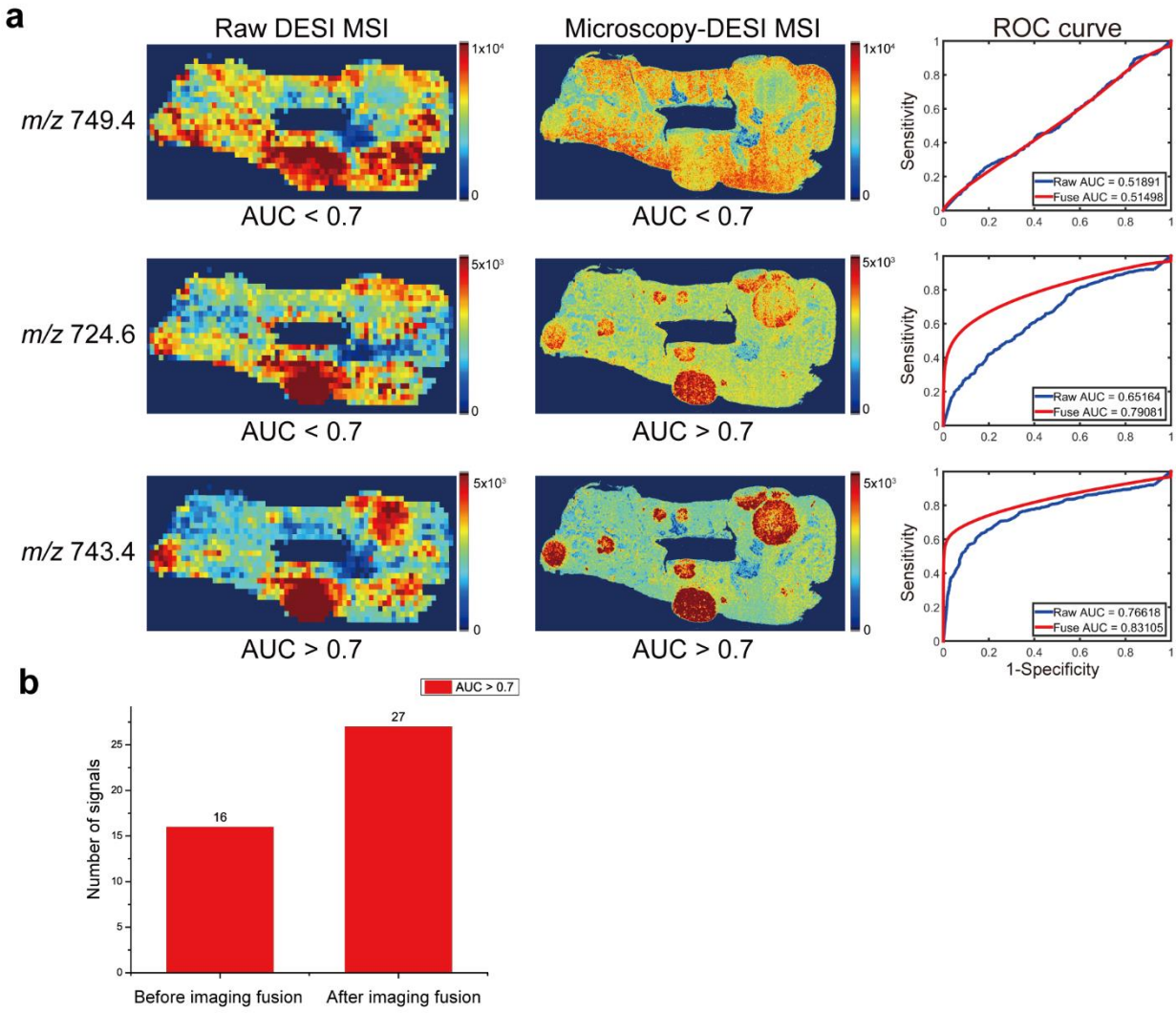


**Fig. 7** Potential biomarker for cancerous tumor margin determination using ROC examination. (a) For *m/z* 749.4, AUC was lower than 0.7 before and after image fusion. For *m/z* 724.6, the AUC was lower than 0.7 before image fusion and higher than 0.7 after image fusion. For *m/z* 743.4, the AUC was higher than 0.7 before and after image fusion. (b) After applying image fusion, number of potential biomarkers (the signals with AUC larger than 0.7) increased by 11.